BUTTERWORTH HEINEMANN

Polymer Vol. 36 No. 1, pp. 73–80, 1995

0032-3861/95/$10.00 + 0.00

Spherulites of *cis*-1,4-polybutadiene: molecular weight effects

Tian-Lai Cheng
Research and Development Department, Taiwan Synthetic Rubber Corp., PO Box 6-11, Kaohsiung, Taiwan 81506, Republic of China

and An-Chung Su*
Institute of Materials Science and Engineering, National Sun Yat-Sen University, Kaohsiung, Taiwan 80424, Republic of China
(Received 26 October 1993; revised 23 May 1994)

Morphological features of melt crystallized *cis*-1,4-polybutadiene were examined by means of polarized light microscopy. Samples similar in branching characteristics but different in molecular weight (MW) were studied. High MW samples exhibited features of dwarf spherulites. Samples of lower MW formed spherulites of radial texture at low crystallization temperatures (T_c), spherulites of banded texture at intermediate T_c, and spherulites of complex birefringence at the high T_c end. Microscopic observations during subsequent heating of the latter spherulites indicated that they were composed of a mainframe of the banded texture and interstitial crystallites with different orientation. The interstitial crystallites melted at a lower temperature range whereas the mainframe persisted to higher temperatures. The melting temperature of slowly cooled or cold-crystallized samples decreased first but then remained approximately constant with increasing MW. These observations are discussed in terms of the entanglement effects during melt crystallization.

(Keywords: *cis*-1,4-polybutadiene; molecular weight effects; crystallization)

INTRODUCTION

The role of chain entanglement in transport properties of polymer melts is well known[1–3]. Crystallization of a polymer in its melt state involves transport and rearrangement of entangled chains in the vicinity of the crystal front[4]. Chain entanglement should therefore play a significant role in the melt crystallization of polymers. This has been explicitly expressed to explain results of bulk crystallization kinetics[5], the apparent Gaussian behaviour of melt crystallized chains[6], and the premelting phenomenon of polymer crystals[7,8]. In a more recent analysis, Robelin-Souffache and Rault[9] concluded that, except at small supercooling, entanglements persist upon crystallization from the melt state. They proposed further that the competition between crystal growth and chain reptation determines the transition between regimes I and II. A theoretical analysis based on the trapping of entanglements was then provided to explain the observed correlation[9] between the long period (L) of the crystallites and the chain size (i.e. radius of gyration) in the melt and the well-known variation of L with supercooling.

In view of the increased reptation time with branch length[3], more apparent entanglement effects are expected in the melt crystallization of polymers with long branches. In a previous study[10], morphological features of spherulites of long-chain branched *cis*-1,4-polybutadiene (cPBD) were examined. The cPBD samples used were similar in molecular weight but different in branching level. It was observed that samples of lower branching levels exhibited typical spherulitic morphology. The spherulites were of banded texture at higher crystallization temperatures (T_c); the band period decreased with decreasing T_c and eventually became unidentifiable as the radial texture emerged. The spherulitic growth rate decreased significantly with increasing level of branching. The most dramatic effect of long-chain branching was manifested by the surge of small ('dwarf') spherulites in the case of highly branched cPBD. The dwarf spherulite stopped growing at a size of several micrometres and induced new dwarf spherulites along its periphery. The process repeated itself to the apparent end of crystallization. The melting temperature of slow-cooled or cold-crystallized samples decreased with increasing level of branching. These observations were discussed in terms of the entanglement concept. In particular, the formation of dwarf spherulites was attributed to the balance between forces of crystallization and rubber-like elasticity for the entangled chains at the crystal front.

It may be argued that, since reptation rate also increases with increasing molecular weight (MW), the effects of long-chain branching observed above should have parallel analogies in cPBD samples of increasing MW. As a natural extension of the previous work, spherulitic features of cPBD samples similar in branching characteristics but different in MW are reported in this paper.

* To whom correspondence should be addressed

EXPERIMENTAL

Materials

Six cPBD samples were synthesized via coordination polymerization in benzene at a fixed temperature of 50°C (to maintain a common level of branching) by use of a homogeneous Co/Al catalyst system. The *MW* was controlled by varying the amount of an externally added chain transfer agent (1,5-cyclo-octadiene). These cPBD samples were ca. 96–97% in *cis*-configuration according to infra-red spectroscopic analysis[11] and were designated as M1 to M6 in order of increasing *MW*. Summarized in *Table 1* are characteristics of these samples determined by means of infra-red spectroscopy, gel permeation chromatography (g.p.c., using tetrahydrofuran as the carrier solvent), and solution viscometry (in toluene). Due to the lack of proper cPBD standards, the g.p.c. results were used to estimate polydispersity index (M_w/M_n) only. Values of weight-average molecular weight (M_w) in *Table 1* were calculated (with corrections[12] for polydispersity effects) from the intrinsic viscosity data by use of published values[13] of Mark–Houwink–Sakurada parameters.

Differential scanning calorimetry

General thermal behaviour of the cPBD samples was studied by means of differential scanning calorimetry (d.s.c.) using a Perkin–Elmer DSC7 instrument. The calorimeter was routinely calibrated using an indium standard. Each sample was equilibrated at 70°C for 3 min and then quickly (ca. -320°C min^{-1}) cooled to -140°C, followed by three to-and-fro scans between -140 and 70°C with the rate of heating or cooling fixed at 20°C min^{-1}.

Polarized light microscopy

Specimens approximately 20–30 μm in thickness were prepared by casting a drop of the 2% toluene solution on a glass slide, followed by drying under vacuum for 1 h at 100°C. An optical microscope (Nikon OPTIPHOT-POL) equipped with a Linkam THMS-600 heating stage connected to a TMS-91 temperature controller and a CS-196 liquid-nitrogen cooling system was used. The specimens were heated to and maintained at 70°C for 3 min, followed by quenching (at a rate of ca. 150°C min^{-1}) to the respective crystallization temperatures (T_c) where morphological observations were made. In the melting experiment, morphological changes of the isothermally crystallized sample during heating at a rate of 1°C min^{-1} were recorded.

RESULTS

General thermal behaviour

Thermograms of the dynamic d.s.c. scans are shown in *Figure 1*. Results of the d.s.c. analysis are summarized in *Table 2*. The six samples exhibit essentially the same glass transition temperature (T_g) at ca. -100°C. In the first heating scan (*Figure 1a*), an endothermic peak (T_{c1}) corresponding to cold crystallization may be observed for the four lower-*MW* samples above T_g; the cold crystallization peak is absent for the two high-*MW* samples, indicating nearly complete crystallization during the fast cooling process. A melting peak (T_{m1}) is generally observed at a temperature slightly lower than 0°C. It is noted that T_{c1} (when present) and T_{m1} tend to decrease with increasing *MW*; this effect, however, levels off in the high-*MW* range.

In the second (cooling) scan (*Figure 1b*), a single crystallization peak is observed for the four higher-*MW* samples; for the two low-*MW* samples, this crystallization peak is either entirely absent (M1) or appears as a slight wiggle in the base line (M2). When observable, the peak temperature of crystallization (T_{c2}) increases with *MW*. The crystallization in the four lower-*MW* samples is apparently incomplete since a cold crystallization peak

Table 2 Summary of dynamic d.s.c. scans

Sample code	T_{c1} (°C)	T_{m1} (°C)	T_{c2} (°C)	T_{c3} (°C)	T_{m3} (°C)
M6	–[a]	−6.9	−38.8	–[a]	−7.0
M5	[a]	−7.5	−48.8	–[a]	−7.5
M4	−46.3	−6.4	−51.3	−55.6	−6.7
M3	−42.5	−2.1	−57.5	−54.4	−2.4
M2	−33.1	−2.2	–[a]	−36.9	−1.8
M1	−28.8	−0.5	–[a]	−32.5	−0.1

[a] Absence of well-defined crystallization peak

Table 1 Characteristics of cPBD samples

	M1	M2	M3	M4	M5	M6
$[\eta]^a$ (dl g^{-1})	0.44	1.02	1.62	2.23	2.99	4.98
$M_w/M_n{}^b$	1.8	1.8	2.0	2.6	2.1	2.1
10^{-4} $M_w{}^c$	2.5	7.9	15.2	24.4	35.6	71.9
$\eta_{5\%}{}^d$ (mPa s)	3.0	8.5	15.2	80.2	223	1450
Microstructure[e]						
cis- (mol%)	95.7	96.5	97.0	96.4	96.1	96.1
trans- (mol%)	2.8	1.9	1.9	1.9	2.1	2.2
vinyl (mol%)	1.6	1.6	1.1	1.7	1.8	1.8

[a] Intrinsic viscosity in toluene at 30°C
[b] Polystyrene-equivalent values from gel permeation chromatography (room temperature, styrogel columns, differential refractive index detector) using tetrahydrofuran as the carrier solvent
[c] Calculated from published values[13] of Mark–Houwink–Sakurada parameters
[d] Viscosity of 5 wt% toluene solution at 25°C, measured by use of a no. 400 Cannon-Fenske viscometer
[e] From infra-red spectroscopic analysis[11]

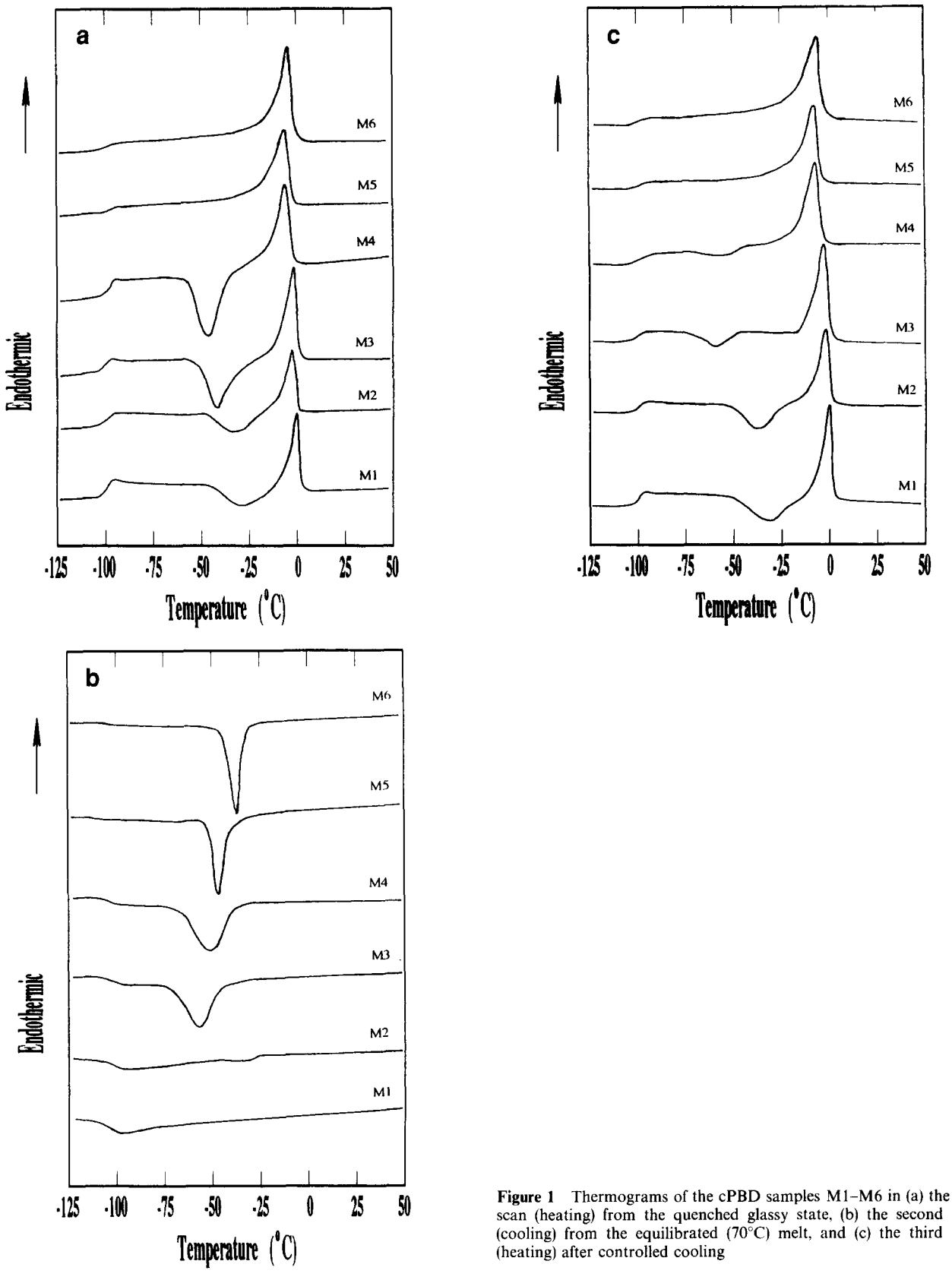

Figure 1 Thermograms of the cPBD samples M1–M6 in (a) the first scan (heating) from the quenched glassy state, (b) the second scan (cooling) from the equilibrated (70°C) melt, and (c) the third scan (heating) after controlled cooling

(T_{c3}) above T_g may be observed in the following heating scan (*Figure 1c*), which also decreases with increasing *MW*. It appears that the higher-*MW* samples crystallize more readily. The final melting temperature (T_{m3}) also decreases first but then remains approximately constant with increasing *MW*. In fact, values of T_{m1} and T_{m3} are nearly identical for a given sample, in spite of the difference (most clearly in the case of M3) in the crystallization temperature range.

Spherulitic morphology

Typical cPBD spherulites, grown isothermally at different temperatures, are shown in *Figures 2* and *3*. The spherulites are optically negative. At smaller supercooling

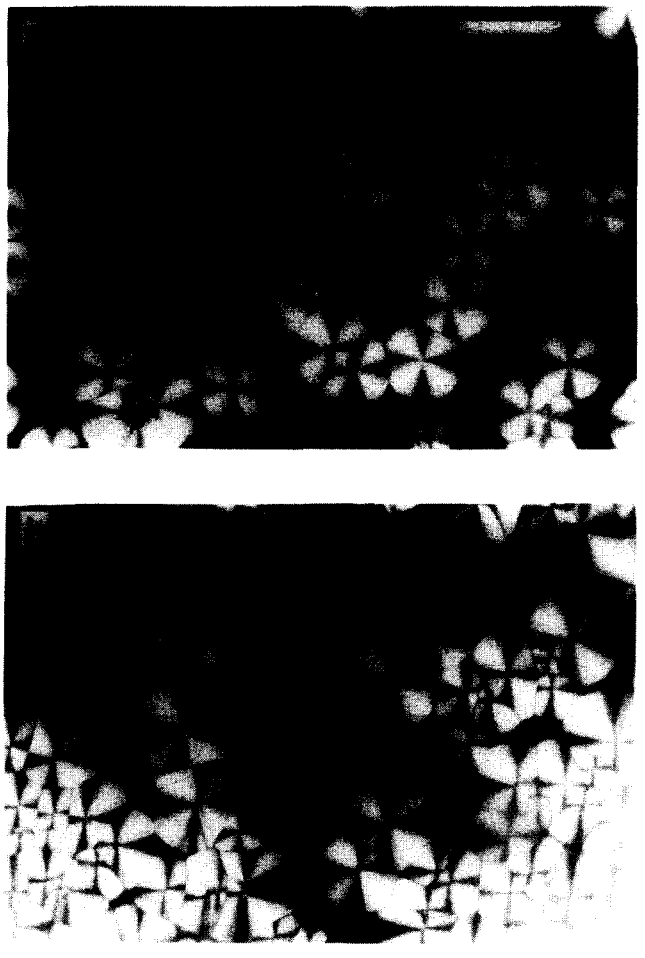

Figure 2 Spherulites formed during isothermal crystallization of M3, observed under cross-polarization after (a) 12 min at −27.5°C and (b) 6.5 min at −35°C. The scale bar corresponds to 50 μm

(*Figure 2a*), banded texture may be observed. The band period decreases with increasing supercooling and becomes unidentifiable in the vicinity of $T_c \approx -35$°C, resulting in radial spherulites (*Figure 2b*). In the case of high-*MW* samples (*Figure 3*), dwarf spherulites may be observed. These morphological features are very similar to those reported in our previous study[10] of branching effects. More interesting features are observed in the case of lower-*MW* samples at relatively low supercooling. Shown in *Figure 4* are coarsely banded M2 spherulites. A further decrease in supercooling results in spherulites of barely recognizable periodicity (*Figure 4c*); the spherulitic texture (i.e. the Maltese cross and the periodic banding) becomes hardly resolvable at the small supercooling end (*Figure 5*).

Clues to the origin of the poorly resolved texture were found from observations during the melting of these spherulites. Shown in *Figure 6a* are M1 spherulites with a messy optical texture and without the Maltese cross (or at most with a slight hint of its presence), indicating non-uniform orientation of crystallites. As the temperature is increased, both periodic banding and Maltese cross begin to appear (*Figures 6b* and *c*) and become most clearly identifiable just before the final melting (*Figure 6d*). These observations suggest the existence of two populations of crystallites: the high-melting crystallites, showing the typical banded texture, correspond to the mainframe of the spherulite; the low-melting crystallites, showing different orientation from the mainframe, fill the interstitial space. This is consistent with the two-morphology model proposed earlier by Bassett and Hodge[14]. The observations above may be summarized as a morphology map given in *Figure 7*.

Growth rate

Due to the peculiar features of dwarf spherulites described above, the spherulitic growth rate (G) of the two high-*MW* samples could not be accurately determined. Logarithmic growth rates of the four lower-*MW* spherulites at various T_c are shown in *Figure 8*. These curves are parabolic in shape, with the maximum located in the vicinity of −50°C. The growth rate decreases with increasing *MW*, in spite of differences in the spherulitic texture. The trend is in contrast to the earlier observation that the higher-*MW* samples are more readily crystallizable during dynamic d.s.c. scans. This can only be explained by the increasing nucleation density with *MW*, as also indicated by results of kinetic analysis of bulk crystallization[15]. One may note that the growth rate curves are not exactly parallel: they tend to shift towards the high T_c end with decreasing *MW*, indicating stronger *MW*-dependence of G at the high T_c range, an effect similarly observed in previous studies[16-18] of linear polymers.

DISCUSSION

Growth rate

The decreasing spherulitic growth rate with increasing *MW* is basically expected, as observed by Magill[19] for poly(tetramethyl-*p*-silphenylene)siloxane and Hoffman *et al.*[20] for polyethylene (PE) fractions. A similar trend has been reported more recently by Lopez and Wilkes[16] for poly(*p*-phenylene sulfide) (PPS), by Cheng *et al.*[17] for poly(ethylene oxide) (PEO) fractions, and by Deslandes *et al.*[18] for poly(aryl ether ether ketone) (PEEK). Qualitatively, the decreased growth rate may be attributed to the decreased chain mobility with increasing *MW*. More specifically, the decrease in chain mobility should be reflected in an increase in reptation time. By identifying the reptation rate with the folding rate in regimes I and II, Hoffman[21] suggested that the spherulitic growth rate should be inversely proportional to *MW*. A later consideration on the free energy change associated with the adsorption of the first stem resulted in a slight modification[22] of the predicted *MW* dependence. The theoretical prediction was in reasonable agreement with previous growth rate data[20] of linear PE fractions in the vicinity of the regime I–II transition. However, observations on other linear polymers[16-18] did not conform to the theoretical prediction.

Within the temperature range studied, the spherulitic growth rate of our lower-*MW* samples decreases by a factor of ca. 0.6 for each three-fold increase in *MW* (i.e. M1 to M2 to M4), weaker than that predicted from the reptation argument of Hoffman. The nearly quenched growth rate (which results in dwarf spherulites of M5 and M6) upon further increase in *MW* cannot be explained by the theory either. The tendency of a weaker effect of long-chain branching than that predicted by a

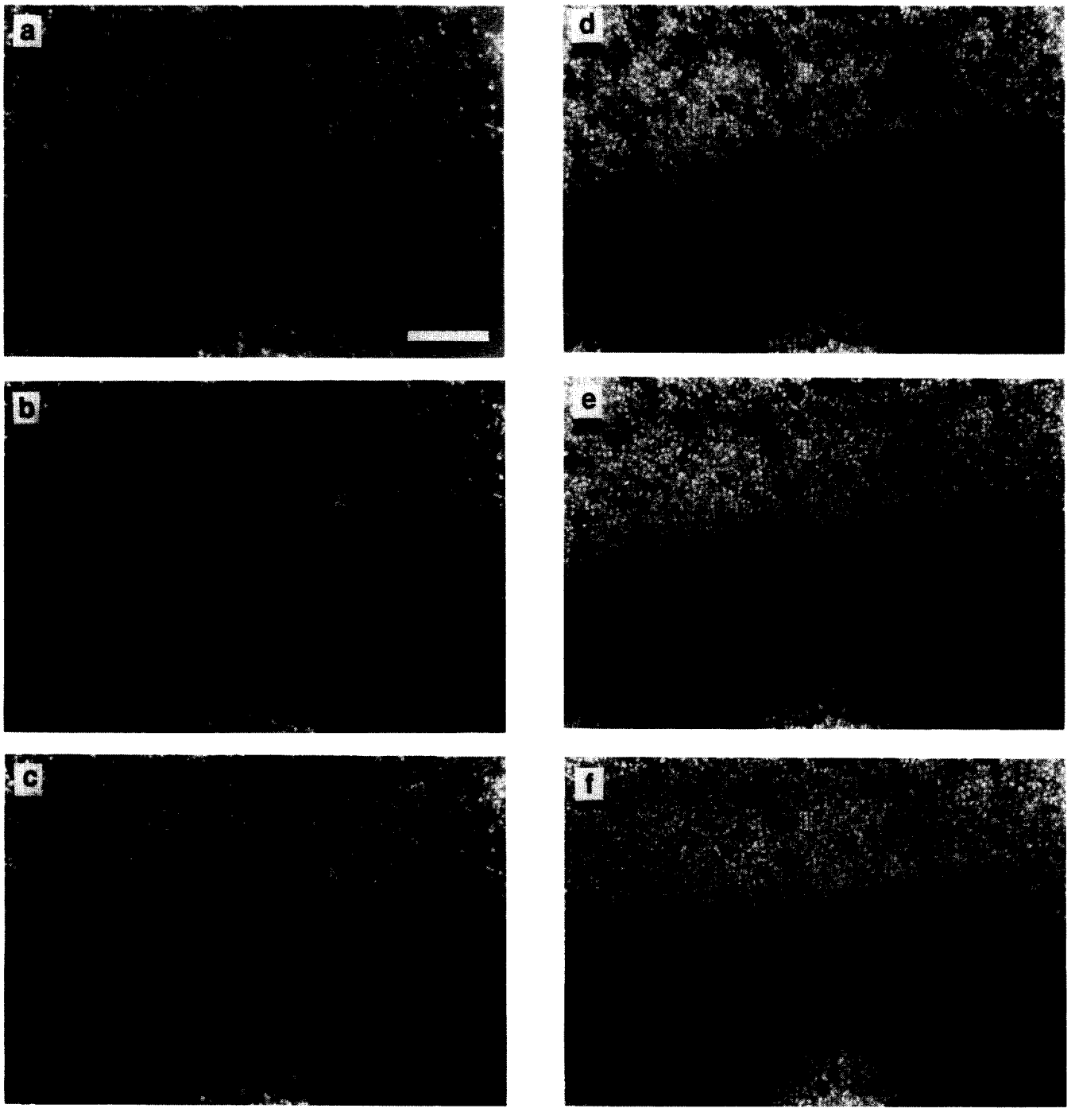

Figure 3 Spherulites formed during isothermal crystallization of M5, observed under cross-polarization after (a) 8 min, (b) 9 min, (c) 10 min, (d) 14 min, (e) 16 min and (f) 18 min at $-27°C$. The scale bar corresponds to 50 μm

simple reptation argument at low branching levels and the nearly complete suppression of growth rate at the high branching end were similarly observed[10]. As proposed previously[10], the weaker-than-predicted dependence on reptation rate may probably be attributed to incomplete disentanglement of the crystallizing chains at the crystal front and hence a mechanistic departure from the Hoffman–Lauritzen picture[23] of melt crystallization. In the extreme case of a very low reptation rate, the folding of a chain (as driven by the crystallization force) attached to the crystal front no longer results in the pull-out of the chain from the melt pool but, instead, deforms the entangled rubbery matrix nearby. The crystallization force is therefore balanced by the rubber elasticity force, resulting in strongly suppressed growth rate. The strained network near the crystal front may subsequently induce primary nucleation (due to alignment of stretched chains), resulting in the observed phenomenon of dwarf spherulites. This does not exclude the commonly accepted view that stress at the growth front may lead to the development of non-crystallographic branching; however, the growth of the branched lamellae should suffer the same suppression. The key factors here are the nearly complete suppression of growth and the

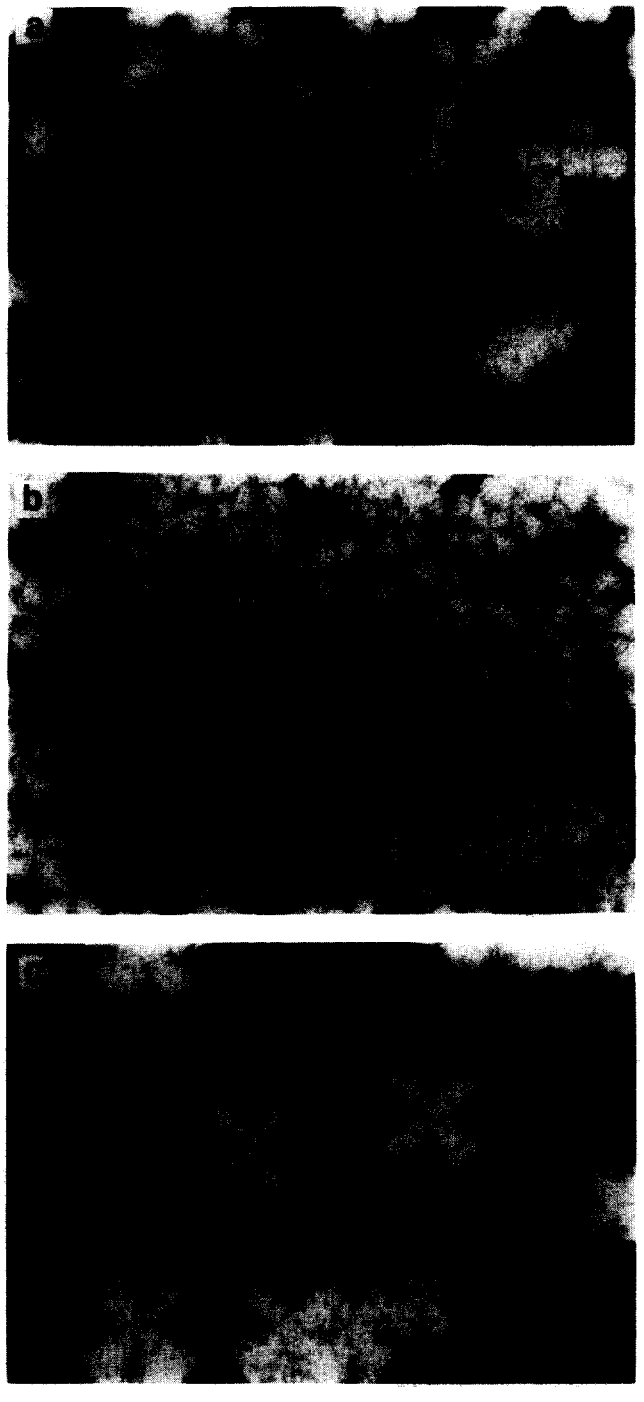

Figure 4 Spherulites formed during isothermal crystallization of M2, observed under cross-polarization after (a) 5.5 min at −32°C, (b) 9.5 min at −32°C and (c) 42.5 min at −25°C. The scale bar corresponds to 50 μm

stronger tendency towards primary nucleation, which in combination allow for the development of dwarf spherulites. The strongly quenched growth rate for the high *MW* cPBD samples here is due mainly to the long-chain branched nature which is known[3] to quench reptation rate. In the case of linear polymers, there are no previous reports of dwarf spherulites for other diene polymers (such as polyisoprenes), but features similar to dwarf spherulites may be identified (see Figure 2 in ref. 18) for high-*MW* PEEK, which is much lower in chain flexibility.

Figure 5 Spherulites formed during isothermal crystallization of M3, observed under cross-polarization after 106 min at −20°C. The scale bar corresponds to 50 μm

Spherulitic texture

The present observation indicates dissipation of band texture at the low-T_c end (i.e. large supercooling) via diminishing band period with increasing growth rate. This is rather similar to the case of PE[24]. Banded spherulites are believed to consist of lamellae twisting[24–28] or curving[29] in concert along the radial direction. The concerted twisting or curving of lamellae has been attributed[30] to the asymmetric stresses set up within disordered fold surfaces. The origin of the asymmetric stresses is not exactly clear but, in our opinion, may probably be related to the elasticity of the entangled chains at the crystal front. At small supercooling (i.e. high T_c), disentanglement is comparatively more complete, resulting in lower stresses and hence a lower frequency of lamellar twisting. With decreasing T_c, disentanglement becomes increasingly difficult, resulting in a higher elastic force on the lamellae and a higher frequency of twisting. This is also consistent with the observations that band period tends to decrease with increasing *MW* (*Figure 9*) at a given T_c. In this sense, the radial texture may be considered to have 'superfine' bands. A closer look at the cPBD spherulites of radial texture indeed indicated hints of very fine bands.

Melting

The decreasing melting temperature (T_{m3}) with increasing *MW* and the insensitivity of T_{m3} to the crystallization temperature range deserve some comments. Similar observations have been reported[10] for cPBD samples of different branching levels. As commented previously[10], these observations may be attributed to the melting–reorganization–remelting mechanism[31–36]. In terms of this model, chains of higher mobility (i.e. lower *MW* or lower level of branching) should be capable of reorganization up to a higher temperature during the d.s.c. scan and therefore should exhibit a higher final melting temperature. Consequently, for a given sample, the difference in lamellar thickness (and therefore the melting temperature) due to the difference in the crystallization temperature range should be smeared by the reorganization process during the d.s.c. scan; the nearly constant value of T_{m3} then simply reflects the

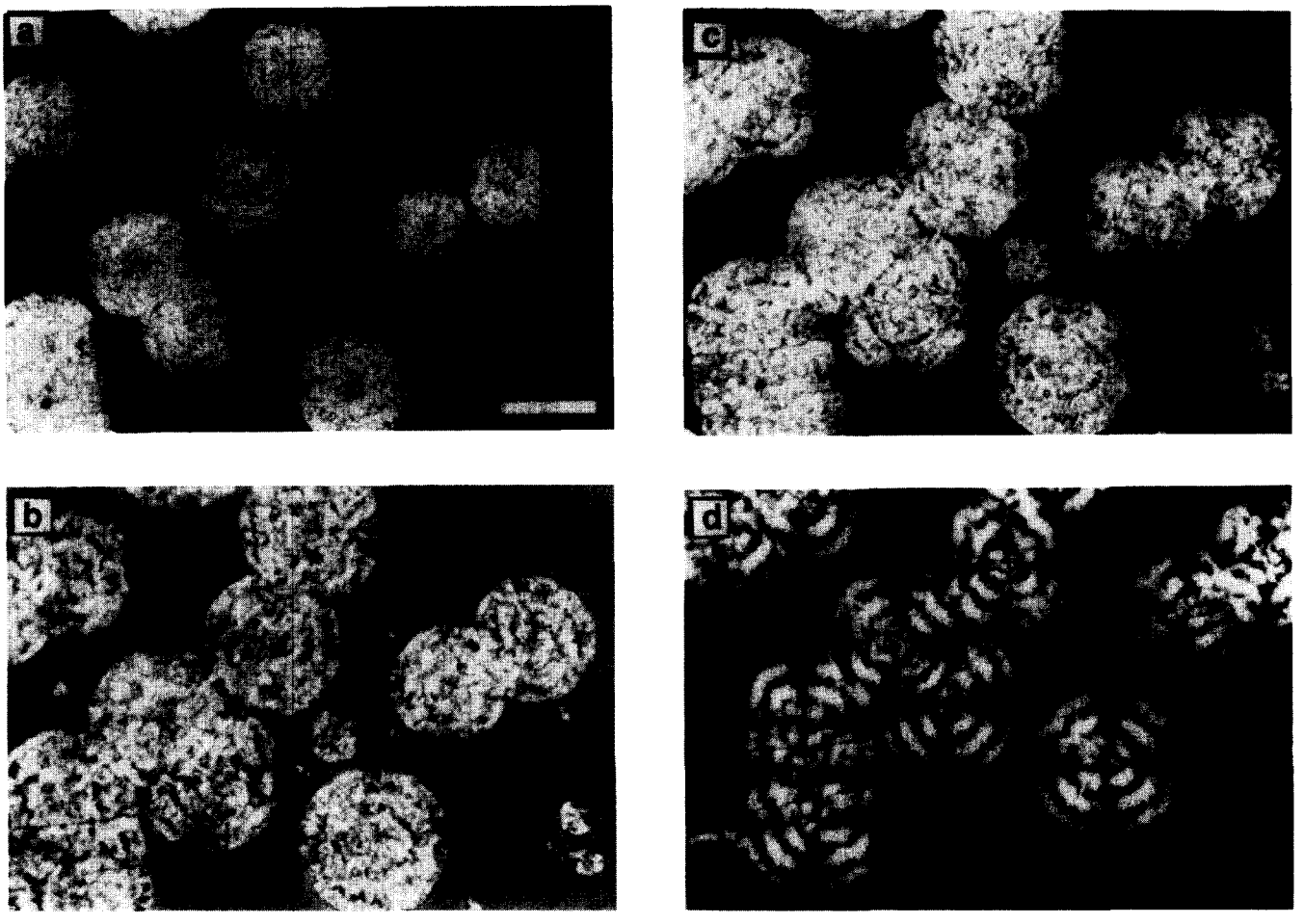

Figure 6 Spherulites formed during isothermal crystallization of M1, observed under cross-polarization: (a) isothermally crystallized for 17 min at −25°C; (b) isothermally crystallized for 30 min at −25°C and then heated at a rate of 1°C min^{-1} to −12°C; (c) heated to −7°C; (d) heated to −2°C. The scale bar corresponds to 50 μm

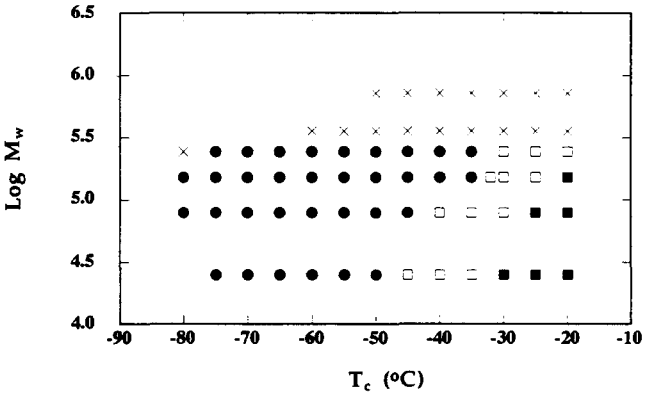

Figure 7 Morphology map for cPBD of different MW at the present branching level: dwarf (×), radial (●), banded (□) and optically messy (■) spherulites

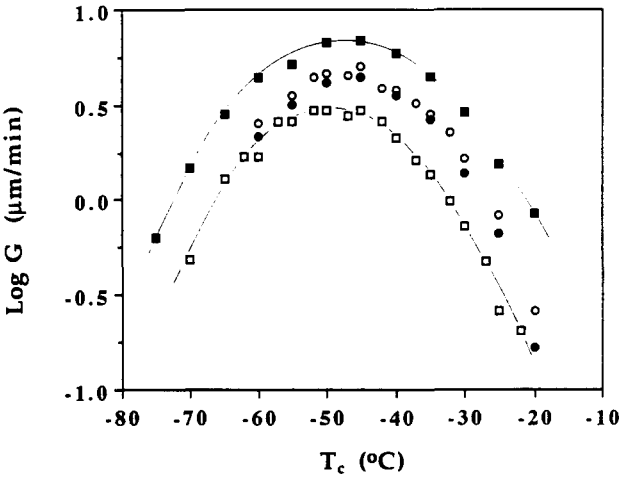

Figure 8 Spherulitic growth rate of M1 (■), M2 (○), M3 (●) and M4 (□) at various crystallization temperatures

high-temperature end of the competing reorganization process at the present heating rate.

On the other hand, our microscopic observations here do indicate the presence of two types of crystals of separate orientations and melting temperatures, in accordance with the dual-population mechanism proposed more recently[37-39]. This model is consistent with the dual-morphology picture of spherulitic structure proposed earlier by Bassett and co-workers[14,40]. In terms of the dual-morphology model, we may attribute the final melting peak to the dominant lamellae which, developed first during spherulitic growth, are comparatively thick and melt at a higher temperature. The melting temperature of the space-filling, subsidiary lamellae is comparatively

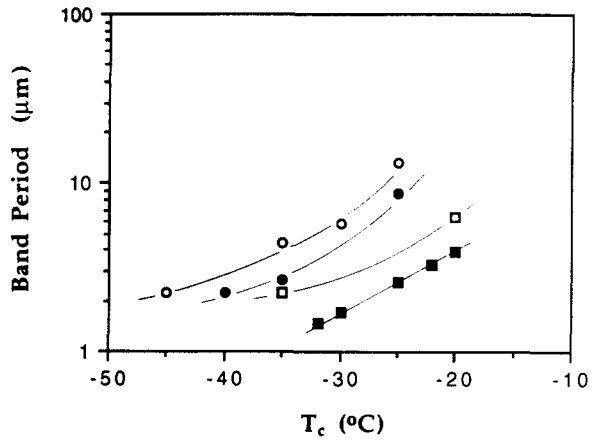

Figure 9 Variation of band period with T_c and MW for M1 (○), M2 (●), M3 (□) and M4 (■)

low and varies more significantly with T_c. In the present case of steady cooling, the melting of subsidiary lamellae is likely to spread over a relatively wide temperature range due to the wide crystallization temperature range involved. This would explain the apparent absence of the melting endotherm for subsidiary lamellae. The model would then suggest that lamellar thickness of the dominant lamellae decreases with MW (or, in the previous case, with long-chain branching). This, along with the observation that the melting temperature of the dominant lamellae (i.e. T_{m3} here) is insensitive to T_c, would require more involved interpretations; this will be discussed in a future report[41] along with more extensive observations on the melting behaviour of cPBD. It suffices to state here that neither of the two mechanisms can be completely eliminated; in fact, both mechanisms can be effective, depending on the crystallization temperature range and the d.s.c. heating rate, as indicated in earlier studies of PEEK[39,42] and PPS[43].

CONCLUSIONS

In summary, we have presented spherulitic features of melt crystallized cPBD samples of different MW but similar branching level at different crystallization temperatures. The general trends observed previously in texture evolution and the formation of 'dwarf' spherulites with decreasing chain mobility were basically reproducible in the present sample series. Interestingly, spherulites of lower-MW samples at high crystallization temperatures exhibited messy birefringence, originating from the coexistence of two populations of crystallites with different melting temperature range. The high melting mainframe lamellae exhibited banded texture whereas in-filling low-melting crystallites exhibited different optical orientation from the mainframe crystallites. In addition, the melting temperature of slow-cooled or cold-crystallized samples decreased with increasing MW but the effect levelled off in the high-MW range. These observations were discussed in terms of the entanglement concept.

ACKNOWLEDGEMENTS

Thanks are due to Mr Chia-Ting Chung at IMSE for his help in the polarized light microscopy study. This work is financially supported by the National Science Council, Republic of China under contract number NSC83-0405-E110-015.

REFERENCES

1 Graessley, W. W. *Adv. Polym. Sci.* 1976, **16**, 1
2 Graessley, W. W. *Adv. Polym. Sci.* 1982, **47**, 67
3 de Gennes, P. G. 'Scaling Concepts in Polymer Physics', Cornell University Press, Ithaca, 1979
4 Wunderlich, B. 'Macromolecular Physics', Academic, New York, 1976, Vol. 2
5 Banks, W., Gordon, M., Roe, R.-J. and Sharples, A. *Polymer* 1963, **4**, 41
6 Calvert, P. *J. Polym. Sci., Polym. Phys. Edn* 1979, **17**, 1341
7 Mansfield, M. L. *Macromolecules* 1987, **20**, 1384
8 Rieger, J. and Mansfield, M. L. *Macromolecules* 1989, **23**, 3810
9 Robelin-Souffache, E. and Rault, J. *Macromolecules* 1989, **22**, 3581
10 Cheng, T. L. and Su, A. C. *Macromolecules* 1993, **26**, 7161
11 Silas, R. S., Yates, J. and Thornton, V. *Anal. Chem.* 1959, **31**, 529
12 Kurata, M. and Tsunashima, Y. in 'Polymer Handbook', 3rd Edn (Eds J. Brandrup and E. H. Immergut), Wiley, New York, 1989, p. VII/1
13 Danusso, F., Moraglio, G. and Gianott, G. *J. Polym. Sci.* 1961, **51**, 475
14 Bassett, D. C. and Hodge, A. M. *Proc. R. Soc.* 1981, **A377**, 25, 39, 61
15 Cheng, T. L. and Su, A. C. unpublished results, 1992
16 Lopez, C. L. and Wilkes, G. L. *Polymer* 1988, **29**, 106
17 Cheng, S. Z. D., Chen, J. and Janimak, J. J. *Polymer* 1990, **31**, 1018
18 Deslandes, Y., Sabir, F.-N. and Roovers, J. *Polymer* 1991, **32**, 1267
19 Magill, J. H. *J. Appl. Phys.* 1964, **35**, 3249
20 Hoffman, J. D., Frolen, L. J., Ross, G. S. and Lauritzen, J. I. Jr *J. Res. Natl Bur. Stand.* 1975, **A79**, 671
21 Hoffman, J. D. *Polymer* 1982, **23**, 656
22 Hoffman, J. D. and Miller, R. L. *Macromolecules* 1988, **21**, 3038
23 Hoffman, J. D., Davis, G. T. and Lauritzen, J. I. Jr in 'Treatise in Solid State Chemistry' (Ed. H. B. Hannay), Plenum, New York, 1975, Vol. 3, Ch. 7
24 Keith, H. D. and Padden, F. J. Jr *Polymer* 1984, **25**, 28
25 Keller, A. *J. Polym. Sci.* 1955, **17**, 291
26 Keller, A. and Wills, H. H. *J. Polym. Sci.* 1959, **39**, 151
27 Keith, H. D. and Padden, F. J. Jr *J. Polym. Sci., Polym. Phys. Edn* 1987, **25**, 2371
28 Lustiger, A., Lotz, B. and Duff, T. S. *J. Polym. Sci., Polym. Phys. Edn* 1989, **27**, 561
29 Bassett, D. C. and Hodge, H. D. *Polymer* 1978, **19**, 469
30 Bassett, D.C. in 'Morphology of Polymers' (Ed. B. Sedlacek), de Gruyter, New York, 1986, p. 47
31 Wunderlich, B. 'Macromolecular Physics', Academic, New York, 1980, Vol. 3
32 Rim, P. B. and Runt, J. P. *Macromolecules* 1983, **16**, 762
33 Blundell, D. J. and Osborn, B. N. *Polymer* 1983, **24**, 953
34 Lee, Y. and Porter, R. S. *Macromolecules* 1987, **20**, 1336
35 Blundell, D. J. *Polymer* 1987, **28**, 2248
36 Nichols, M. E. and Robertson, R. E. *J. Polym. Sci., Polym. Phys. Edn* 1992, **30**, 305
37 Cheng, S. Z. D., Cao, M.-Y. and Wunderlich, B. *Macromolecules* 1986, **19**, 1868
38 Cebe, P. and Hong, S.-D. *Polymer* 1986, **27**, 1183
39 Bassett, D. C., Olley, R. H. and Al Raheil, I. A. M. *Polymer* 1988, **29**, 1745
40 Bassett, D. C. and Vaughan, A. S. *Polymer* 1986, **27**, 1472
41 Cheng, T. L. and Su, A. C. manuscript in preparation
42 Kruger, K.-N. and Zachmann, H. G. *Macromolecules* 1993, **26**, 5202
43 Chung, J. S. and Cebe, P. *Polymer* 1992, **33**, 2312